

SCIENTIFIC REPORTS



OPEN

Transformation from Quantum to Classical Mode: the Size Effect of Plasmon in 2D Atomic Cluster System

Reng-lai Wu¹, Jun Quan¹, Chunhua Tian¹ & Mengtao Sun²

On the basis of tight-binding approximation, the energy absorption of 2D atomic clusters is calculated by the linear response theory. Through the energy-absorption peaks in the presence of different external potentials, various types of plasmon modes are specified in clusters with dozens to hundreds atoms, such as transverse dipole plasmon, longitudinal dipole plasmon, transverse quadrupole plasmon, and longitudinal quadrupole plasmon. Moreover, the transformation of plasmon from quantum to classical mode is observed in clusters with different shape and different electron density. The particular transformation process demonstrate that: there are only a few modes of plasmon in clusters with few-atoms; as the number of atoms in cluster is increased, the number of plasmon modes increases, the gaps between plasmon frequencies become smaller, the quantum modes of plasmon gradually evolve into continuous modes, and the dispersion of quantum-mode plasmon gradually transforms into the one of classical 2D plasmon. Such process reveals the size effect of plasmon in 2D clusters, which can be explained by the fact that the energy levels near the Fermi energy are denser and more compact in larger-size clusters.

With the development of nanotechnology and the miniaturization of optoelectronic devices, it has becomes increasingly necessary to explore and better understand the excitation properties of plasmon in nanoclusters. For example, the plasmon biosensor is applied to detect cell pathological changes according to the sensitive interactions between light and nano-scale biological molecules¹. On the other hand, the investigation of the plasmon at the nanoscale is motivated by its applications in nanotechnology and biotherapy areas²⁻⁸. Among the researches on plasmon in nano-structures, classical theory begins to fail in micro system with size less than 10 nanometers, while the quantum effect of plasmon comes to play an important role. which may lead to some distinctive and unusual properties, such as the change of plasmon's frequency and lifetime⁹⁻¹², the blueshifts and redshifts of plasmons' resonances with the increase of nano-system size¹³⁻¹⁷, and different plasmon modes under different electric potentials¹⁸⁻²¹. Much research work has been done to understand the quantum effects of plasmon. Scholl and co-workers used an analytical quantum mechanical model to describe the shift of plasmon frequency¹⁰. Nordlander's team proposed a quantum dynamic scheme to research the influence of quantum effect on the plasma resonance in two separated nanodimers, and found that, as the distance between the two nanodimers is less than 1 nanometer, the enhancement of electromagnetic field would be much smaller than the result predicted by the classical theory¹¹. Applying the time-dependent density functional theory and local density approximation, Gao's team found the transverse and longitudinal plasmon in linear metallic atomic chain, which excited by the electric field along transverse and longitudinal direction, respectively¹²⁻¹⁴. Basing on the linear-response theory and the eigen-equation method, Bertsch, Yu, Xue, *et al.* found lots of plasmon modes in various atomic clusters¹⁸⁻²⁰, interestingly, the earlier experiment carried out by Schlipper had already reported the multiple collective plasmon resonance in the sodium cluster²¹. These studies provide meaningful results for the quantum effect of plasmon, and a lot of them have demonstrated the presence of discrete quantum modes of plasmon in

¹School of Physical Science and Technology, Lingnan Normal University, Zhanjiang, 524048, P.R. China. ²School of Mathematics and Physics, Beijing Key Laboratory for Magneto-Photoelectrical Composite and Interface Science, University of Science and Technology Beijing, Beijing, 100083, P.R. China. Reng-lai Wu and Jun Quan Contributed equally. Correspondence and requests for materials should be addressed to C.T. (email: chunhuatian@lingnan.edu.cn) or M.S. (email: mengtaosun@ustb.edu.cn)

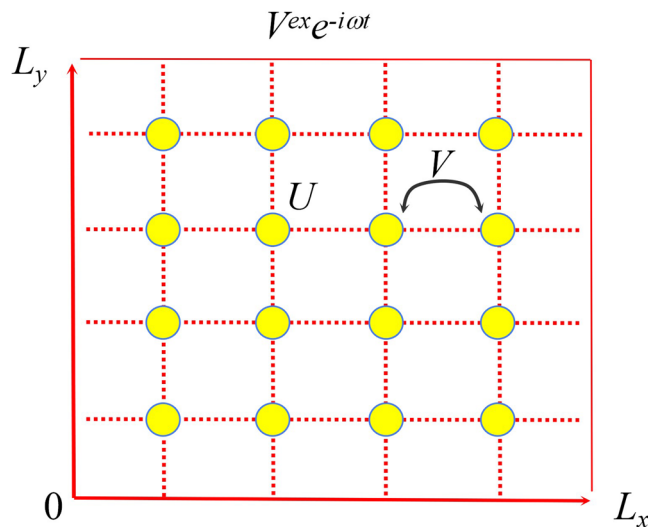


Figure 1. The model of 2D atomic cluster with size $N_x \times N_y = 4 \times 4$.

nano-cluster system^{12–21}. However, the dispersion of quantum-mode plasmon in nano-cluster system is still indistinct, and the transformation process of the plasmon from quantum modes to the classical mode is still unknown.

In this paper, we apply the linear response theory to calculate the energy absorption of plasmon in two dimensional (2D) atomic cluster system. The results reveal that quantum modes of plasmon exist in 2D atomic cluster system. However, the size effect of plasmon arises with changing cluster dimensions and electron density, resulting in a transformation of the quantum-mode plasmon into the classical one as the cluster dimensions grow.

Model and Theory

The model of 2D atomic cluster under study is presented in Fig. 1, where the transverse length $L_x = (N_x + 1)a$, and the longitudinal length $L_y = (N_y + 1)a$. Here, N_x and N_y , respectively, are the atom numbers in the transverse and longitudinal directions, a is the distance between the nearest two atoms. $V^{ex}(\mathbf{l}, \omega)e^{-i\omega t}$ is the time-dependent external electric potential, where, $V^{ex}(\mathbf{l}, \omega)$ is the space distribution of the external potential, $\mathbf{l} = l_x \mathbf{e}_x + l_y \mathbf{e}_y$ is the lattice coordinate, l_x and l_y respectively are components of \mathbf{l} in X and Y directions, \mathbf{e}_x and \mathbf{e}_y respectively are unit vectors in X and Y directions, and ω the frequency of the external potential. U is the on-site Coulomb interaction, and V is the nearest-neighbor Coulomb interactions^{22,23}. In this model, electrons are tightly bound to the lattice points, and can only hop into neighboring lattice points, so the model is suitable for crystals whose lattice constant is much larger than the atom radius.

In the wannier representation, the plasmon excited by $V^{ex}(\mathbf{l}, \omega)e^{-i\omega t}$ can be found by the peaks of energy absorption function:

$$L(\omega) = \frac{1}{2} \omega \operatorname{Im} \left\{ \sum_{\mathbf{l}} [V^{ex}(\mathbf{l}, \omega)] Q(\mathbf{l}, \omega) \right\} \tag{1}$$

where $Q(\mathbf{l}, \omega)$ is the induced charge. Based on the linear response theory and tight-binding approximation, $Q(\mathbf{l}, \omega)$ can be determined by^{17,19}

$$\sum_{\mathbf{l}'} \left[\delta_{\mathbf{l}\mathbf{l}'} - \sum_{\mathbf{l}''} \Pi(\mathbf{l}, \mathbf{l}'', \omega) v_{\mathbf{l}\mathbf{l}''} \right] Q(\mathbf{l}', \omega) = e^2 \sum_{\mathbf{l}'} \Pi(\mathbf{l}, \mathbf{l}', \omega) V^{ex}(\mathbf{l}', \omega) \tag{2}$$

Here, $v_{\mathbf{l}\mathbf{l}'}$ is given by

$$v_{\mathbf{l}\mathbf{l}'} = \begin{cases} \frac{U}{2}, & \mathbf{l}' = \mathbf{l} \\ V, & |\mathbf{l}' - \mathbf{l}| = a \\ 0, & \text{else} \end{cases} \tag{3}$$

and $\Pi(\mathbf{l}, \mathbf{l}', \omega)$ is the Linhard function:

$$\Pi(\mathbf{l}, \mathbf{l}', \omega) = 2 \sum_{mn} \frac{f(E_m) - f(E_n)}{E_m - E_n - \omega - i\eta} \psi_m^*(\mathbf{l}) \psi_n(\mathbf{l}) \psi_n^*(\mathbf{l}') \psi_m(\mathbf{l}') \tag{4}$$

where, $f(E_m)$ is the Fermi function, η is the scattering rate, and $\psi_n(\mathbf{l})$ is the eigenvector corresponding to eigenvalue E_n , which can be written as

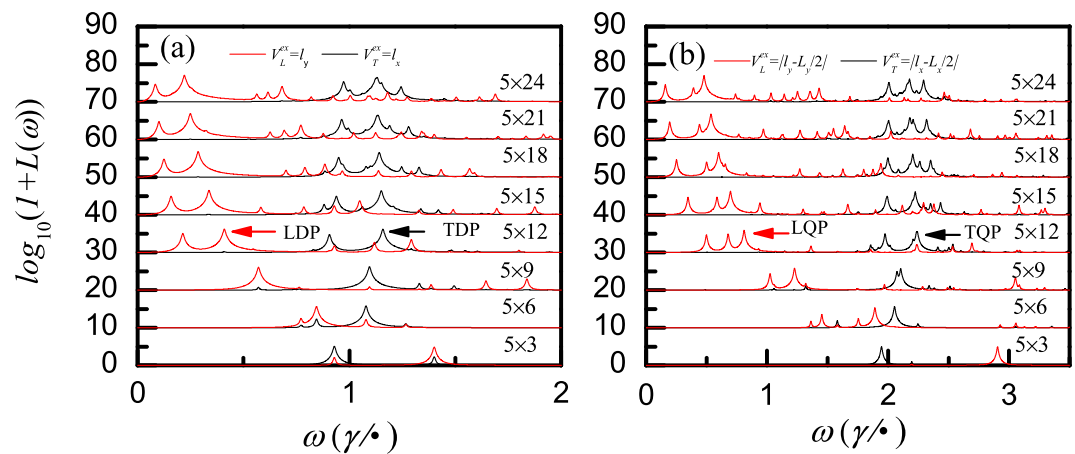


Figure 2. The evolution of energy absorption with the longitudinal size N_y for a fixed transverse size $N_x = 5$, whereas $N_y = 3, 6, 9, 12, 15, 18, 21, 24$ from bottom to top. **(a)** The applied external potentials are $V_T^{ex} = l_x$ and $V_L^{ex} = l_y$; **(b)** The applied external potentials are $V_T^{ex} = |l_x - L_x/2|$ and $V_L^{ex} = |l_y - L_y/2|$. In all clusters the electron density is identical and given by $n_e = 2.133 \times 10^{18} \text{ m}^{-3}$, and $\gamma = 2.0 \text{ eV}$.

$$\psi_n(\mathbf{l}) = \sqrt{\frac{4}{L_x L_y}} \sin\left(\frac{n_x \pi}{L_x} l_x\right) \left(\frac{n_y \pi}{L_y} l_y\right) \quad (5)$$

$$E_n = -2\gamma \cos\left(\frac{n_x \pi}{L_x}\right) - 2\gamma \cos\left(\frac{n_y \pi}{L_y}\right) \quad (6)$$

where, $n_x = 1, 2, 3, \dots, N_x$, $n_y = 1, 2, 3, \dots, N_y$, γ is the nearest-neighbor transfer energy.

Results and Discussions

In all the calculations, we set the parameters that $U = 3.0 \text{ eV}$, $V = 1.0 \text{ eV}$, $\eta = 0.005 \text{ eV}$. The unit of frequency is γ/\hbar , with \hbar the Planck's constant, and that of the space coordinate is the distance a , with $a = 0.4 \text{ nm}$. The size of the system is expressed by $N_x \times N_y$, the face electron density $n_e = N_e/(N_x N_y a^2)$, where N_e is the electron number. V_L^{ex} is the potential of longitudinal electric field which is applied in the y direction; V_T^{ex} is the potential of transverse electric field which is applied in the x direction. Arbitrary units are adopted for the values of the energy absorption and the charge.

Figure 2 shows the transverse-mode (TM) and longitudinal-mode (LM) plasmon in atomic cluster system, where logarithmic coordinate is adopted for the y axis due to very large values of the energy absorption. According to the refs^{12–15,24}, the energy-absorption peaks induced by the longitudinal electric field (see red lines) represent LM plasmon. On the other hand, the energy-absorption peaks induced by transverse electric field (see black lines) represent TM plasmon. In Fig. 2(a), the main LM plasmon (the one with the largest energy absorption) and the sub-main LM plasmon (the one with the second largest energy absorption) shift red with the increase of the longitudinal size, due to reduction of the energy gaps involved in the excitation in large size cluster system. However, the main and sub-main TM plasmon shift blue with the increase of the longitudinal size, which is similar to the behavior of one-dimensional end TM plasmon^{13,14}. Since the external electric fields in Fig. 2(a) are linear, only dipole plasmons can be excited, so the plasmons shown in Fig. 2(a) are longitudinal dipole plasmon (LDP) and transverse dipole plasmon (TDP), respectively. Apart from the usual LDP and TDP, longitudinal quadrupole plasmon (LQP) and transverse quadrupole plasmon (TQP) are also illustrated in Fig. 2(b). It is clear that TQP is excited by the transverse symmetry electric field $V_T^{ex} = |l_x - L_x/2|$, while LQP by the longitudinal symmetry electric field $V_L^{ex} = |l_y - L_y/2|$. In Fig. 2(a,b), the frequency of the main quadrupole plasmon is larger than the one of the main dipole plasmon, it is agreed with the experimental result in refs^{25,26} that the quadrupole resonance are corresponding to higher energy excitation. However, the size dependence of LDP and LQP are similar, the size dependence of TDP and TQP are similar too. While the longitudinal size is very large, the frequencies of the main TDP and TQP have certain values, such behaviour is in agreement with the experimental observation of plasmon in graphene monolayer in the ref.²⁵.

The charge distribution, which is defined by $Q(\mathbf{r}, \omega) = \sum_{\mathbf{l}} Q(\mathbf{l}, \omega) |\phi(\mathbf{l}, \mathbf{r})|^2$ with $\phi(\mathbf{l}, \mathbf{r})$ the s -wave function set to be $\phi(\mathbf{l}, \mathbf{r}) = R_{40}(\mathbf{r} - \mathbf{l}) Y_{00}(\theta, \phi)$, at the main LDP, TDP, LQP, and TQP is presented in Fig. 3. The $4s$ orbit wave function is used here, so the calculation results are suitable for artificial one-layer systems consist of K Ca, Cu or Zn atoms, the valance electrons of which are in the $4s$ orbit. In fact, for one-layer systems consist of Rb, Sr, Ag, Cd, Au, or Hg atoms, the results are similar, due the valance electrons of these atoms are all in the s orbit. At the main LDP and TDP (see Fig. 3(a1,a2), respectively), it shows dipole character along the longitudinal and transverse directions, respectively, whereas at the main LQP and TQP (see Fig. 3(a3,a4), respectively), it manifests symmetric character along the longitudinal and transverse directions, respectively. Moreover, the charge at the main TQP

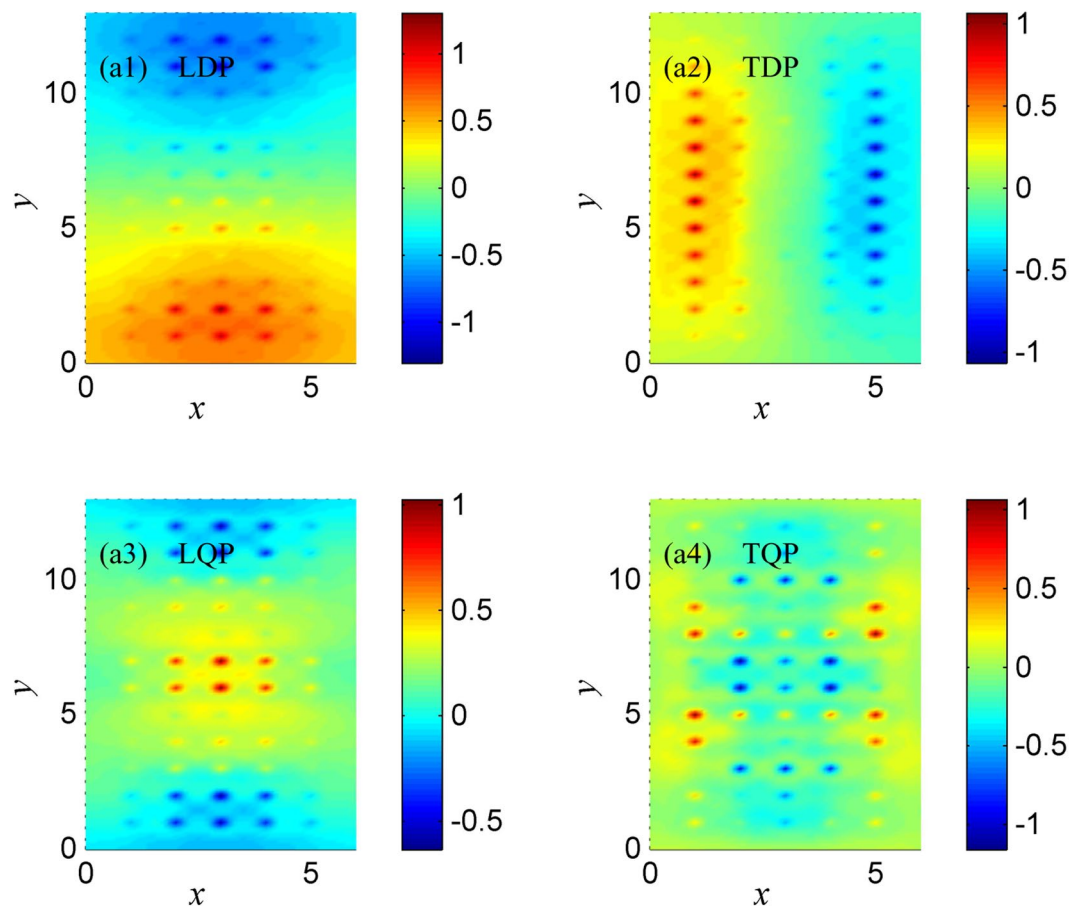


Figure 3. The charge distributions at the main (a1) LDP, (a2) TDP, (a3) LQP, and (a4) TQP. The specific LDP, TDP, LQP, TQP are marked with arrows for system 5×12 involved in Fig. 2, and the corresponding external fields are the same as that in Fig. 2.

also show symmetric character along the longitudinal directions, implying that this TM plasmon can be both excited by transverse and longitudinal symmetry electric fields, as shown by the two energy-absorption peaks at the main TQP in Fig. 2(b). The characteristics of the TM plasmon excited by longitudinal electric field also happens in the systems $N_y = 3, 6$ and 12 in Fig. 2(a), due to the fact that TM plasmon may have dipole character along longitudinal direction.

Normally (or Usually), only the main and sub-main plasmons are interested. However, it is important to take into account the low energy-absorption plasmons in the investigation of the frequency spectra of 2D plasmons, since the low energy-absorption plasmons and the high energy-absorption plasmons together form the spectra of plasmon. In the range of $0-4 (\gamma/\hbar)$, after all the peak frequencies of LDPs in Fig. 2(a) are collected, the frequency spectra of the LDPs is illustrated in Fig. 4(a). In clusters with less than 45 atoms (see the clusters with size smaller than 5×9), the total amount of LDPs is small, and the frequency spectra of LDPs is discrete. As the number of atoms is increased, more LDP modes come to appear in the larger-size systems due to more coupling ways of electrons. Such behavior of plasmon is somewhat analogous to the that of phonon (the quantization of lattice vibration). In addition, with the increase of the atoms, the gaps between plasmon frequencies become smaller, the frequency spectra turn to continuous, and the frequency spectra is decreased. All these changes are mainly caused by the fact that in larger-size system the energy levels near the Fermi energy are denser and thus closer to each other.

In order to gain a deeper understanding of the size effect of plasmon, we illustrate the plasmon dispersions of different-size clusters in Fig. 4(b). And our results are compared with the classical 2D plasmon dispersion $\omega^2 = \left(\frac{2\pi n_e e^2}{m_e} \right) q_s^2 + \frac{3}{4} q_s^2 v_F^2$, where, n_e the face electron density, $v_F = \hbar k_F / m_e$ is the Fermi speed, and k_F the Fermi vector which satisfies $k_F^2 = 2\pi n_e$. Quasi-wave vector q_s is introduced to study how the quantum mode transform to classical one. According to the plasmon frequency spectra, quasi-wave vector is defined by $q_s = (n_p / N_p) q_{max}$ where q_{max} is the maximum value of the wave vector which determined by the equation $\omega_{max}^2 = \left(\frac{2\pi n_e e^2}{m_e} \right) q_{max}^2 + \frac{3}{4} q_{max}^2 v_F^2$, here, ω_{max} is the largest frequency of quantum-mode plasmon which equals to $\omega(N_p)$ of the largest cluster.

For the cluster with few atoms, the quantum modes of plasmon are dispersed in the vicinity of the classical dispersion curve, as illustrated in Fig. 4(b). As the number of atoms is increased, the discrete quasi-wave vector gradually becomes continuous, and the discrete dispersion curve moves closer to the classic dispersion curve.

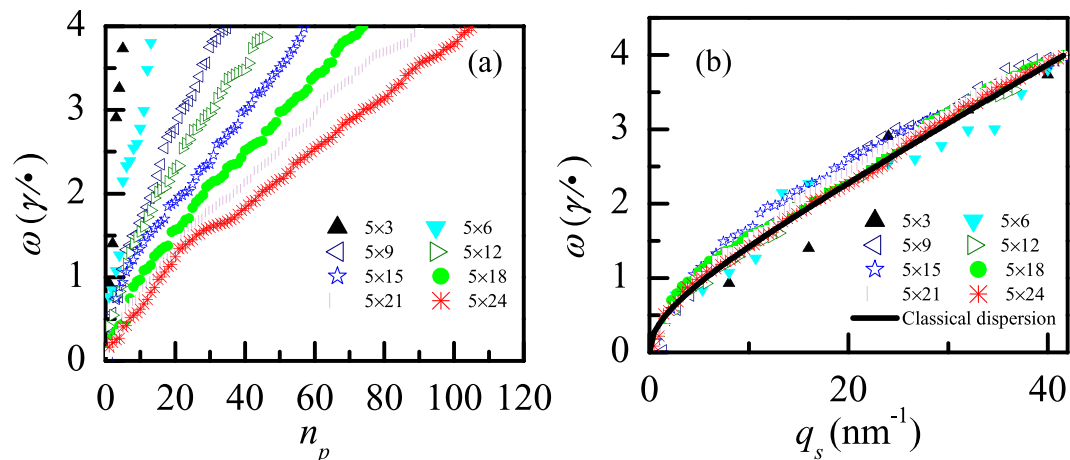


Figure 4. (a) The evolution of frequency spectra of LDPs with size. Here n_p is the number of the plasmon, and given by $n_p = 1, 2, 3, \dots, N_p$, representing that the plasmons are ordered from the lowest to the largest frequency, with N_p the number of the largest-frequency plasmon which is also the total amount of plasmons; (b) The evolution of plasmon dispersion with size for LDPs (scatter symbols), and the dispersion of classical 2D plasmon (continuous line). The corresponding clusters are the same as that in Fig. 2.

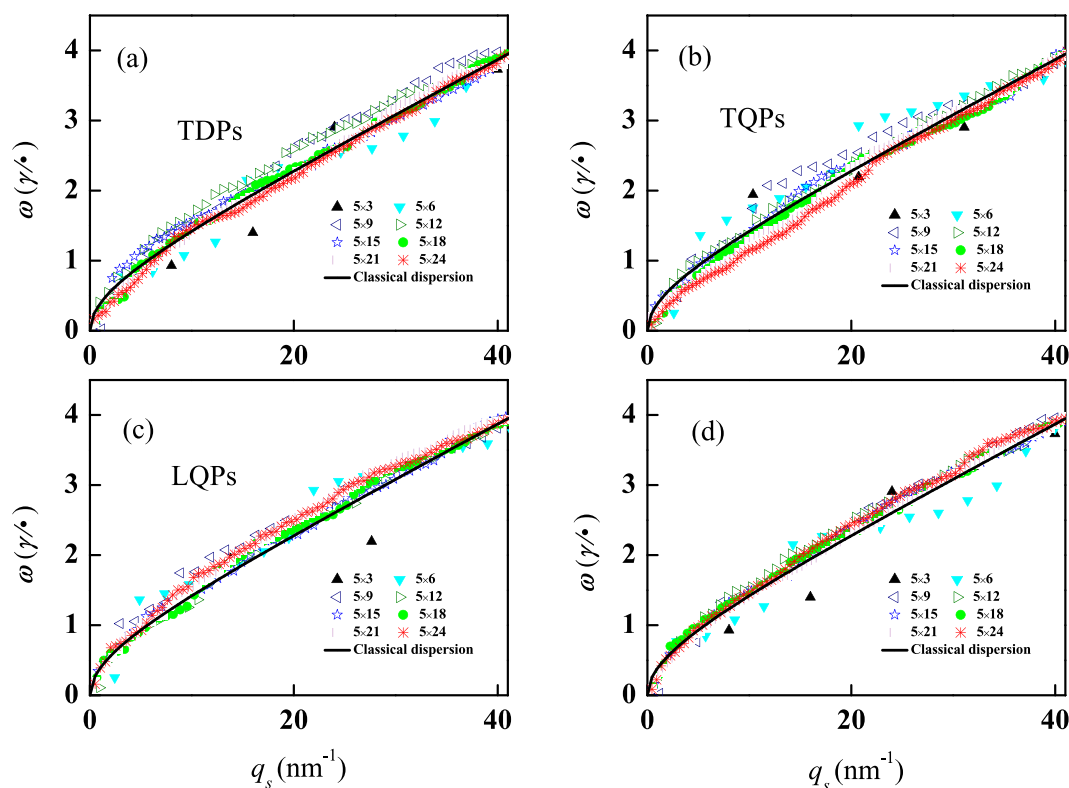


Figure 5. The evolution of plasmon dispersion with size. (a) for TDPs excited by $V_T^{ex} = l_x$; (b) for LQPs excited by $V_L^{ex} = |l_y - L_y/2|$; (c) for TQPs excited by $V_T^{ex} = |l_x - L_x/2|$; (d) for plasmons excited by $V_T^{ex} = l_x + l_y$. The scatter symbols are obtained by the quantum-mode plasmon, and the continuous curves in (a–d) are obtained by the classical 2D plasmon which are the same to each others. The corresponding clusters are the same as that in Fig. 2.

For the cluster with more than 90 atoms (cluster size $N_x \times N_y \geq 5 \times 18$), the dispersions of the quantum-mode plasmon coincide, to a large extent, with that of the classical plasmon. We argue that in this case the quantum mode of plasmon has transformed into the classical one. Such transformation is supported by the Bohr correspondence principle, which states that the behavior of quantum plasmon reproduces classical physics in the large size clusters.

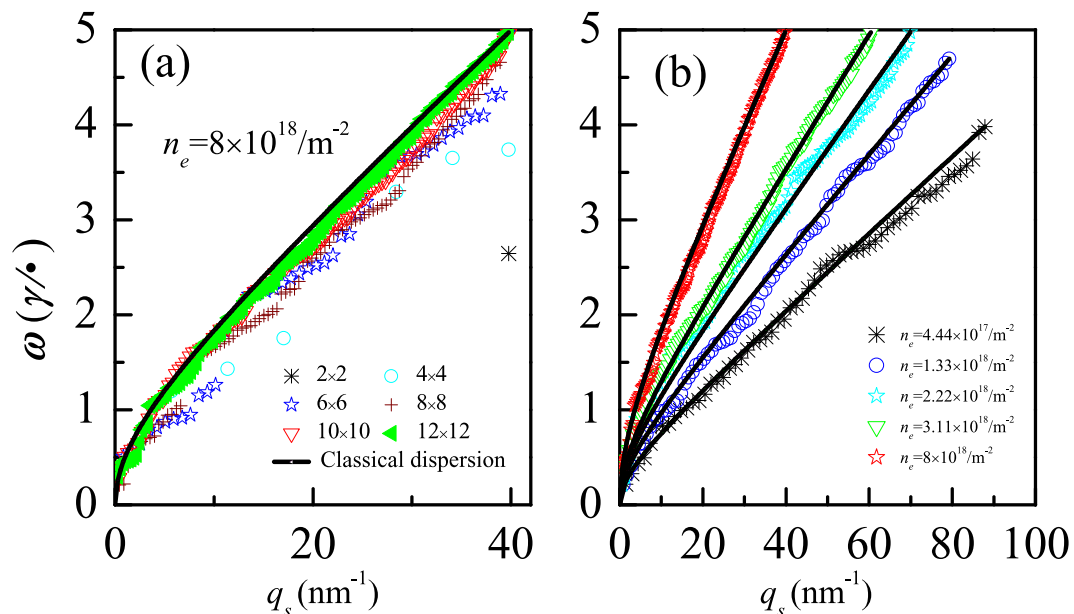


Figure 6. (a) The evolution of plasmon dispersion with size, where all plasmons are excited by $V^{\text{ex}} = I_x + I_y$ (scatter symbols), all clusters are square in shape and are the same in electron density $n_e = 8 \times 10^{18} / \text{m}^{-2}$; (b) The dispersion of plasmons that excited by $V^{\text{ex}} = I_x + I_y$ (scatter symbols) for different electron density, where the cluster size is fixed to be 12×12 , and $\gamma = 3 \text{ eV}$. The electron density of the classical dispersion (continuous curves) equals the one of nearby scatter symbol.

The evolution of plasmon dispersion with size and subject to different external fields are presented in Fig. 5(a–d). In all these four subplots, the dispersion curves of the quantum-mode plasmons display a common feature: they become continuous as the system size grows, and virtually transform into the same dispersion curve, i.e. the dispersion curve of classical 2D plasmon. Therefore the transform property of quantum-mode plasmon is independent on the external fields, as well-known, so does the classical 2D plasmon dispersion. It is worth noting that the main plasmon modes excited by different external fields (see Fig. 2) are not all the same, but they obey the same dispersion relationship in large clusters. So, if the dispersions of quantum-mode plasmon and 2D classical plasmon are coincident, the main plasmons can be found at the corresponding wave vectors in the classical dispersion curve.

In Figs 4 and 5, all clusters are rectangular in shape. Interestingly, for the square-shape clusters in Fig. 6(a), the transformation of plasmon from quantum to classical mode occurs, too, implying that the transformation property of plasmon is unaffected by the shape of 2D cluster. In Fig. 6(b), for the 12×12 cluster with different electron density, the dispersions of quantum-mode plasmon all agree well with that of the classical one. Moreover, the dispersion curve is higher for larger electron density, which indicates that the collective electronic excitations require larger frequencies in larger electron-density system due to more sparse energy levels around higher Fermi energy^{12–15}.

Conclusions

Based on the linear response theory, we have calculated the energy absorption of 2D atomic cluster systems. From the results various types of plasmon excited by electric potentials are specified, such as LDP, TDP, LQP and TQP. Furthermore, through the evolution of quantum-mode plasmon dispersion with size, the transformation property of quantum-mode plasmon is observed in the case of different external fields and in the clusters with different dimensions and different electron density, the transformation property shows a common feature that: more plasmon modes of plasmon exist in atomic cluster with more atoms, with the increase of cluster size, the discrete modes of plasmon will gradually evolve to the continuous one, and the dispersion curve of quantum-mode plasmon will transform into classical plasmon dispersion curve. Such property clarifies the size effect of plasmon in clusters with few atoms.

References

- Abid, A. *et al.* Plasmonic Sensing of Oncoproteins without Resonance Shift Using 3D Periodic Nanocavity in Nanocup Arrays. *Adv. Opt. Mater.* **5**, 1601051 (2017).
- Taylor, A. B. & Zijlstra, P. Single-Molecule Plasmon Sensing: Current Status and Future Prospects. *ACS Sensors* **2**, 1103–1122 (2017).
- Wei, H. *et al.* Quantum dot-based local field imaging reveals plasmon-based interferometric logic in silver nanowire networks. *Nano Lett.* **11**, 471–475 (2011).
- Ma, R. M., Ota, S., Li, Y., Yang, S. & Zhang, X. Explosives detection in a lasing plasmon nanocavity. *Nat. Nanotechnol.* **9**, 600–604 (2014).
- Genevet, P. *et al.* Controlled steering of Cherenkov surface plasmon wakes with a one-dimensional metamaterial. *Nat. Nanotechnol.* **10**, 804–809 (2015).
- Wang, S. M. *et al.* A $14 \times 14 \mu\text{m}^2$ footprint polarization-encoded quantum controlled-NOT gate based on hybrid waveguide. *Nat. Commun.* **7**, 11490 (2016).

7. Zhang, Y. *et al.* Sub-nanometre control of the coherent interaction between a single molecule and a plasmonic nanocavity. *Nat. Commun.* **8**, 15225 (2017).
8. Sun, M. *et al.* Remotely excited Raman optical activity using chiral plasmon propagation in Ag nanowires. *Light: Sci. & Appl.* **2**, e112 (2013).
9. Mortensen, N. A. *et al.* A generalized non-local optical response theory for plasmonic nanostructures. *Nat. Commun.* **5**, 3809 (2014).
10. Scholl, J. A., Koh, A. L. & Dionne, J. A. Quantum plasmon resonances of individual metallic nanoparticles. *Nature* **483**, 421–427 (2012).
11. Zuloaga, J., Prodan, E. & Nordlander, P. Quantum description of the plasmon resonances of a nanoparticle dimer. *Nano Lett.* **9**, 887 (2009).
12. Yan, J., Yuan, Z. & Gao, S. Emergence of collective plasmon excitation in a confined one-dimensional electron gas. *Phys. Rev. Lett.* **98**, 216602 (2007).
13. Yuan, Z. & Gao, S. Plasmon resonances in linear atomic chains: free-electron behavior and anisotropic screening of d electrons. *Phys. Rev. B* **78**, 1879–1882 (2008).
14. Yan, J., Yuan, Z. & Gao, S. End and central plasmon resonances in linear atomic chains. *Phys. Rev. Lett.* **98**, 216602–216605 (2007).
15. Liu, D. D., Zhang, H. & Cheng, X. L. Plasmon resonances and electron transport in linear sodium atomic chains. *J. App. Phys.* **112**, 788–435 (2012).
16. Muniz, R. A., Haas, S., Levi, A. F. J. & Grigorenko, I. Plasmonic excitations in tight-binding nanostructures. *Phys. Rev. B* **80**, 1132–1136 (2009).
17. Wu, R., Quan, J. & Sun, M. Influence of the external field on the excitation properties of plasmon in linear atomic chain. *Sci. Rep.* **8**, 12563 (2018).
18. Bertsch, G. F., Bulgac, A., Tománek, D. & Wang, Y. Collective plasmon excitations in C60 clusters. *Phys. Rev. Lett.* **67**, 2690 (1991).
19. Xue, H. J., Wu, R. L., Hu, C. X. & Zhang, M. The study of the plasmon modes of square atomic clusters based on the eigen-oscillation equation of charge under the free-electron gas model. *Int. J. Mod. Phys. B* **32**, 1850139 (2018).
20. Yu, Y. Q., Yu, Y. B., Xue, H. J., Wang, Y. X. & Chen, J. Plasmon excitations in two-dimensional atomic cluster systems. *Physica B* **496**, 26–33 (2016).
21. Schlipper, R., Kusche, R. & Haberland, I. H. Multiple excitation and lifetime of the sodium cluster plasmon resonance. *Phys. Rev. Lett.* **80**, 1194–1197 (1997).
22. Chui, S. T. & Bray, J. W. Computer renormalization group calculation of the $2k_F$ and $4k_F$ correlation functions of an extended one-dimensional Hubbard model. *Phys. Rev. B* **21**, 1380–1384 (1980).
23. Bray, J. W. & Chui, S. T. Computer renormalization-group calculations of $2k_F$ and $4k_F$ correlation functions of the one-dimensional Hubbard model. *Phys. Rev. B* **19**, 4876–4882 (1979).
24. Moaied, M., Palomba, S. & Ostrikov, K. Quantum plasmonics: longitudinal quantum plasmons in copper, gold, and silver. *J. Optics* **19**, 10 (2017).
25. Zhu, X. *et al.* Experimental observation of plasmons in a graphene monolayer resting on a two-dimensional subwavelength silicon grating. *Appl. Phys. Lett.* **102**, 131101 (2013).
26. Raza, S. *et al.* Multipole plasmons and their disappearance in few-nanometre silver nanoparticles. *Nat. Commun.* **6**, 8788 (2015).
27. Stern, F. Polarizability of a Two-Dimensional Electron Gas. *Phys. Rev. Lett.* **18**, 546–548 (1967).

Acknowledgements

The work is supported by NSF of China Grants (Grant No: 11647156, 11704169, 201502085, 11304276, 61674073, 91436102 and 11374353), the Natural Science Foundation of Guangdong Province, China (Grant No: 2017A030313022, 2017A030307015, 2015A020211038) and the Fundamental Research Funds for the Central Universities in China.

Author Contributions

M.S. and C.T. supervised the project. R.W. and J.Q. performed calculations and analyzed the data. R.W., J.Q. and M.S. wrote the paper.

Additional Information

Competing Interests: The authors declare no competing interests.

Publisher's note: Springer Nature remains neutral with regard to jurisdictional claims in published maps and institutional affiliations.



Open Access This article is licensed under a Creative Commons Attribution 4.0 International License, which permits use, sharing, adaptation, distribution and reproduction in any medium or format, as long as you give appropriate credit to the original author(s) and the source, provide a link to the Creative Commons license, and indicate if changes were made. The images or other third party material in this article are included in the article's Creative Commons license, unless indicated otherwise in a credit line to the material. If material is not included in the article's Creative Commons license and your intended use is not permitted by statutory regulation or exceeds the permitted use, you will need to obtain permission directly from the copyright holder. To view a copy of this license, visit <http://creativecommons.org/licenses/by/4.0/>.

© The Author(s) 2019